Supporting Information

Title
Soft, Implantable Bioelectronic Interfaces for Translational Research

Authors
Dr. Giuseppe Schiavone[1], Florian Fallegger[1#], Dr. Xiaoyang Kang[1#], Beatrice Barra[2], Dr. Nicolas Vachicouras[1], Evgenia Roussinova[1], Ivan Furfaro[1], Dr. Sebastien Jiguet[1], Dr. Ismael Seáñez[3], Simon Borgognon[2,3], Andreas Rowald[3], Dr. Qin Li[5,6], Prof. Chuan Qin[5], Dr. Erwan Bézard[5,6,7,8], Prof. Jocelyne Bloch[3,4], Prof. Grégoire Courtine[3,4#], Dr. Marco Capogrosso[2#], Prof. Stéphanie P. Lacour[1]*

[1]Bertarelli Foundation Chair in Neuroprosthetic Technology, Laboratory for Soft Bioelectronics Interface, Institute of Microengineering, Institute of Bioengineering, Centre for Neuroprosthetics, Ecole Polytechnique Fédérale de Lausanne, 1202 Geneva, Switzerland
[2]Department of Neuroscience and Movement Science, University of Fribourg, 1700 Fribourg, Switzerland
[3]Center for Neuroprosthetics and Brain Mind Institute, School of Life Sciences, École Polytechnique Fédérale de Lausanne, 1015 Lausanne, Switzerland
[4]Defitech Center for Interventional Neurotherapies (NeuroRestore), Department of Neurosurgery, University Hospital of Lausanne (CHUV) and University of Lausanne (UNIL) 1011 Lausanne, Switzerland
[5]Institute of Lab Animal Sciences, China Academy of Medical Sciences, 100021 Beijing, China
[6]Motac Neuroscience Ltd, SK10 4TF Manchester, UK
[7]Institut des Maladies Neurodégénératives, University of Bordeaux, UMR 5293, Bordeaux, France
[8]CNRS, Institut des Maladies Neurodégénératives, UMR 5293, Bordeaux, France
[#]Equally contributing authors

*Prof. Stéphanie P. Lacour, corresponding author
EPFL Campus Biotech, LSBI, Chemin des mines 9, 1202 Geneva, Switzerland
E-mail: ((stephanie.lacour@epfl.ch))

Silicone-on-Silicon (SoS) process for the fabrication of soft electrode arrays

Implants are prepared in a class 100 cleanroom environment by using a combination of microfabrication processes adapted to soft materials on 4" silicon wafers. The devices are fabricated by processing two identical silicone layers, each 170 – 220 μm thick, hereinafter referred to as substrate and encapsulation carriers, which are subsequently covalently bonded together. All silicone layers are prepared by mixing PolyDiMethylSiloxane (PDMS, Sylgard 184, Dow Corning) using a weight ratio of 10:1 between pre-polymer and cross-linker. The PDMS layers are cured for a minimum of 3 hours in a temperature-controlled convection oven set to 75°C. The total thickness of the implants ranges around 350 – 450 μm, which we have found to offer both ease of handling by the surgeon and good fit into the non-human primate (NHP) epidural space. A step by step cross section diagram of the process flow is available in **Figure S1**, accompanied by descriptions and parameters listed in **Table S1**.

Fabrication of the soft insertion tool

The soft insertion tool is fabricated from a polyimide foil core (Kapton HN, DuPont, USA) overmolded with silicone elastomer (Elastosil 2145 10:1, Wacker, Germany). A 125 μm thick polyimide foil is machined with a femtosecond laser (Optec laser micro machining systems MM200-USP) to cut the outline of the core and the holes for better silicone flow through the core. The holes made along the polyimide core are 0.5 mm in diameter, except for the tips, where larger holes (1 mm diameter) are included to facilitate threading the suture wire. The polyimide foil is dipped in adhesion promoter (Primer 1200-OS, Dow Corning, USA) for better adhesion to the silicone overmold, then dried in air. A 3D-printed Acrylonitrile Butadiene Styrene mold coated with an anti-adhesion layer (NeverWet, Rust-Oleuum, USA) is used for the silicone overmolding. The silicone base and crosslinker are mixed to a 10:1 weight ratio and the mix is subsequently degassed. A first thin layer of silicone is poured manually into the mold, then the polyimide core is placed in the mold and finally the top silicone is poured. The excess silicone over the mold is removed with a blade. The assembly is cured in an oven at 80°C for 2 hours. After this, the mold is removed from the oven and the insertion tool is extracted from the mold.

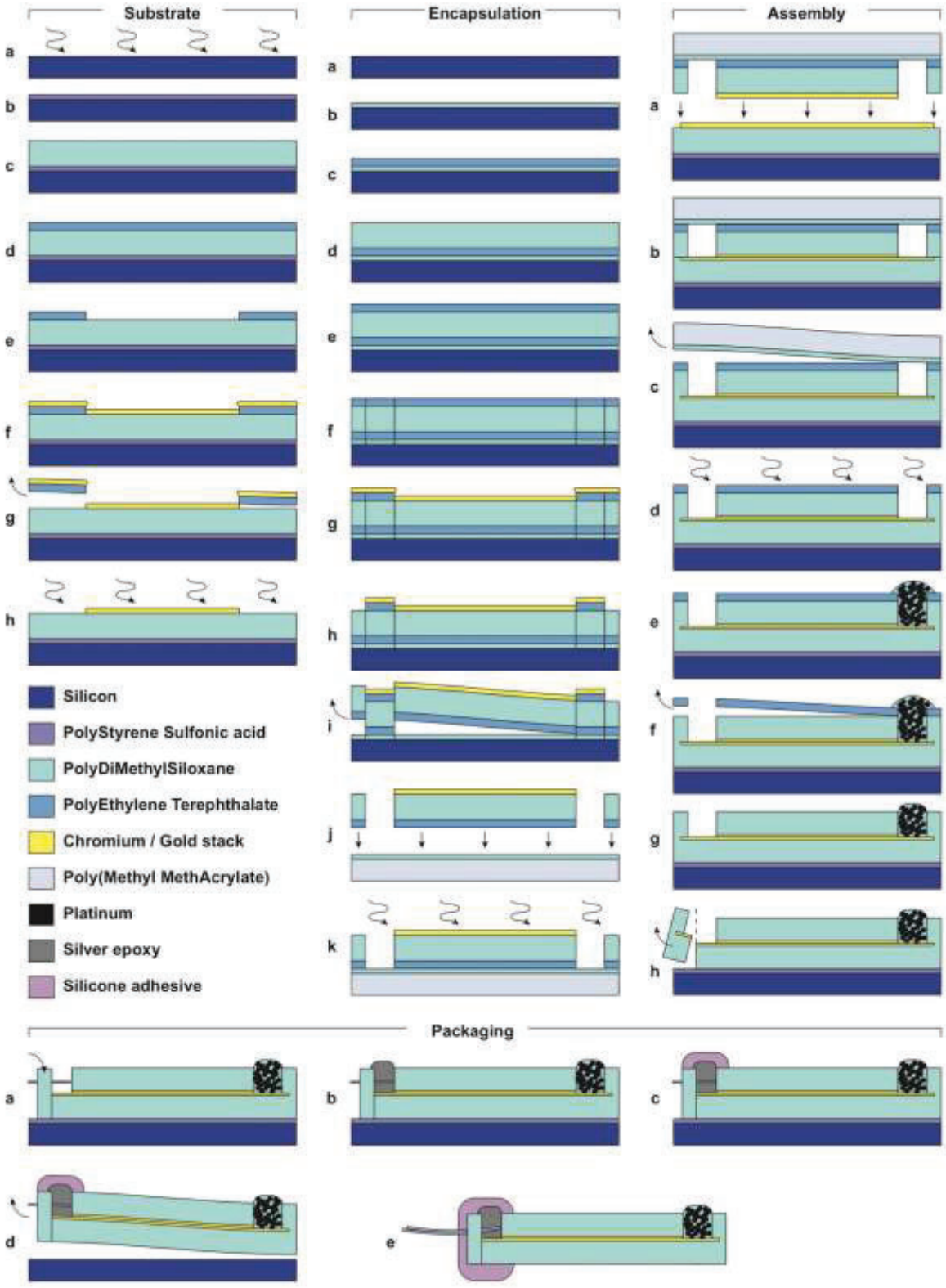

Figure S1 – Cross-section diagram of the SoS process flow for the fabrication of soft implants. Each step of the process is described in **Table S1**.

Electrical characterization of e-dura wiring

A close-up photograph of the wire-to-track transition with the soft machined connector and conductive epoxy prior to sealing with the silicone adhesive is provided in **Figure S2a**. Ad-hoc Kelvin bridge test structures were fabricated within the SoS process and the 4 terminals connected with conductive Ag paste to loose wires (**Figure S2b,c**). The electrical resistance of a gold track was measured continuously using the 4-wire (4W) and 2-wire (2W) techniques for about 30 seconds using a Keithley 2400 SMU, sampling values at 6 Hz. The difference between the means of the two measurements was used as estimation of the transfer resistance (we assumed the wire resistance negligible). The values obtained on 3 samples are illustrated in **Figure S2d**. The results indicate that the ohmic contribution of the wiring assembly is negligible compared to the resistance of the thin-film gold tracks.

We have additionally evaluated the cross-talk between adjacent tracks on an implant by comparing the track-to-track impedance with the open-circuit impedance, where the counter and reference leads of the potentiostat are connected to a track on the electrode sample and the working electrode is left disconnected (in air). The curves show that the modulus of the impedance measured between adjacent tracks is capacitive in nature and lower than the open-circuit impedance (parasitic), but orders of magnitude higher than the typical impedance modulus across the spectrum measured in solution or *in vivo*. This result suggests that for this specific 3D device geometry, the effect of crosstalk (i.e. stimulation through channels adjacent to the selected one) is negligible.

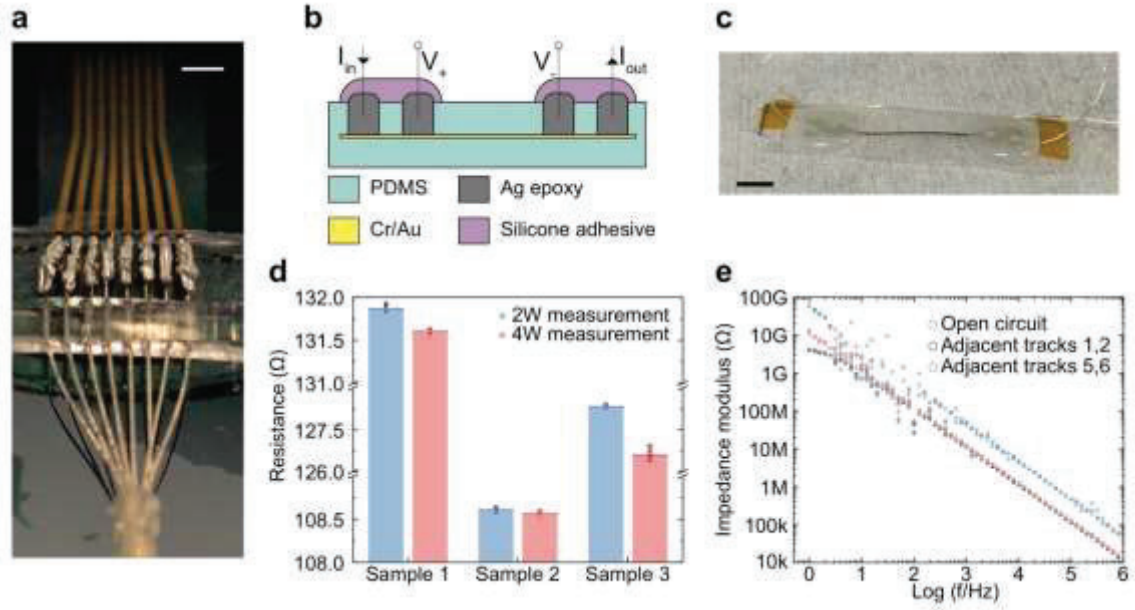

Figure S2 – *e-dura* wiring, electrical transfer resistance and insulation. (**a**) Photograph of the soft connector holding the wire assembly aligned with the interconnect pads. Scale bar: 2 mm. (**b**) Cross-section diagram and (**c**) photograph of a test structure used to characterize the transfer resistance between wires and the gold interconnect. Scale bar: 5 mm. (**d**) Difference between 4W and 2W resistance measurements used to evaluate the transfer resistance between wires and the Au interconnect. Bar height: mean. Horizontal bar: median. n > 300 measurements for all samples. (**e**) Impedance modulus comparison between the open circuit parasitic (working electrode: open; counter and reference electrodes: one of the implant tracks) and adjacent tracks on an implant (e.g. working electrode: track 1; counter and reference electrodes: track 2) in air.

Anatomical 3D reconstructions from Computed Tomography (CT) and Magnetic Resonance Imaging (MRI)

We acquired high resolution mixed-contrast MRI images of the lumbosacral and cervical spinal cords of rats (post mortem) and non-human primates (in vivo) in order to visualize the soft tissues located in the spinal canal of each species. Non-human primates were sedated and imaged in a clinical 3T MRI (Discovery MR750, GE Healthcare, Waukesha, WI) using a standard 8-channel knee coil. The rodent spinal cord was imaged post-mortem in a 9.4T horizontal MRI system (Magnex Scientific, Abingdon, UK), equipped with a 12-cm internal diameter gradient coil insert and interfaced to a DirectDrive console (Varian, Palo Alto, CA) using a custom-made radio frequency coil. We segmented the white matter and cerebrospinal fluid (CSF) in both animal species from the acquired images using the iSeg software developed by ZMT (www.zurichmedtech.com). Non-human primates underwent CT scans to image the bony vertebral structures. A three-point registration technique then enabled the alignment of CT and MRI datasets. The anatomical contours of the grey matter were extracted from a spinal atlas (pages 324 – 338 in the supporting information reference [1]), and scaled by a factor corresponding to the size ratio of the white matter between the MRI segmentation and the spinal atlas. The segmented datasets were imported into the Sim4Life software (ZMT, www.zurichmedtech.com), where volumes were generated. The epidural fat tissue was automatically created by Boolean subtraction between the bone and CSF. The 3D volumes resulted from these computational reconstructions capture the anatomical structures of the spine and spinal cord in rats and non-human primates.

In vitro electrochemical characterization

Electrochemical Impedance Spectroscopy (EIS)

EIS measurements were taken in vitro by immersing the array under test in a beaker containing Phosphate Buffered Saline solution (Gibco PBS, pH 7.4, 1X), along with a platinum wire as counter electrode and a Ag|AgCl reference electrode (Metrohm, El. Ag/AgCl DJ RN SC: KCl). In this 3-electrode configuration, electrochemical impedance spectra were acquired at room temperature using a Gamry Instruments Reference 600 potentiostat (100 mV amplitude, 1 Hz – 1 MHz frequency). A typical EIS measurement is shown in **Figure S3**.

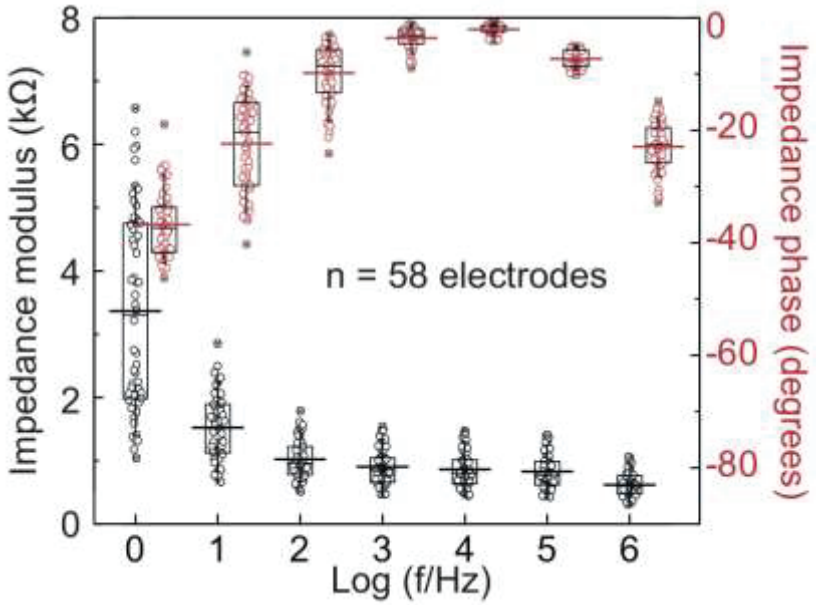

Figure S3 – Electrochemical impedance spectrum of a batch of electrodes (GSA: 0.014 cm^2). Black data points: impedance modulus, left axis. Red data points: impedance phase, right axis. n = 58 electrodes, box band: second quartile, whiskers: 10-90%, horizontal bars: mean.

Voltage Transients (VT), Charge Injection Capacity (CIC) and minimum cathodic polarization

In the same 3-electrode configuration as for EIS measurements, VT curves were acquired following constant current pulsing to measure the polarization properties of the electrodes. Current-controlled, symmetric, biphasic, charge balanced, cathodic-leading pulses were applied between the electrode under test (working electrode) and the Pt counter electrode

using an A-M Systems Model 3800 Pulse Stimulator (0.3 ms per phase pulse width, 1 s inter-pulse period, 0.06 ms inter-phase delay), while measuring the voltage across the working and reference electrodes with an oscilloscope (MDO3014 Mixed Domain Oscilloscope, Tektronix).

VT measurements are used to estimate the cathodic CIC of Pt-PDMS electrodes *in vitro*. The electrode polarization at the onset of the charge-balancing anodic phase of the stimulation pulse (0.3 + 0.06 ms after the onset of the cathodic phase) is monitored to evaluate the polarization of the electrode-electrolyte interface. The difference between the inter-pulse potential and voltage measured at the end of the inter-phase delay is an estimate of the interface polarization, excluding the access voltage that is instantaneously dropped across the resistive parts of the circuit (interconnect, electrolyte, cables). The cathodic CIC limit is evaluated by gradually increasing the stimulation amplitude, until observing an interface polarization of -0.6 V, corresponding to the cathodic boundary of the water electrolysis window for platinum versus Ag|AgCl.[2] This maximal current, divided by the electrode GSA (0.014 cm^2 in this study), is a measure of the cathodic CIC limit of the electrode under test. Further details of the CIC measurements shown in **Figure 2f** for varying electrode size are illustrated in **Figure S4**.

VT measurements are also used to estimate the minimum cathodic polarization arising from current-controlled pulse stimulation. This quantity, noted as E_{min}, is relative to a specific stimulation amplitude and pulse width and can be measured as the minimum electrode polarization recorded with a voltage transient measurement. The minimum cathodic polarization is a metric that enables to estimate the voltage requirements needed to deliver the desired stimulation pulse through an electrode, either *in vitro* or *in vivo*.

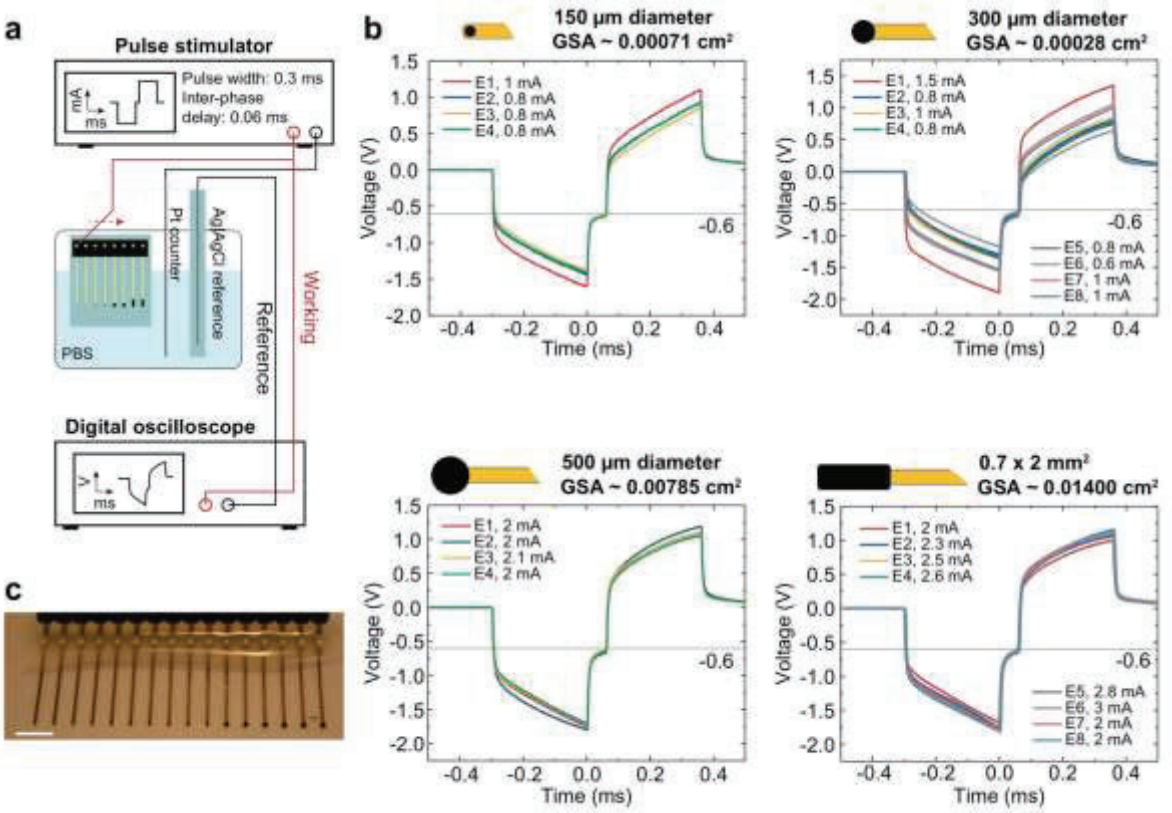

Figure S4 – Voltage transient measurements for the charge injection capacity estimation. (**a**) Measurement setup. A multi-electrode array with electrodes of different GSAs is tested in PBS in a three-electrode configuration. A pulse stimulator delivers current-controlled pulses between the working electrode and a platinum counter electrode. A digital oscilloscope is used to measure the working electrode polarization against an Ag|AgCl reference. (**b**) Voltage transients for different electrode sizes at current amplitudes producing a cathodic interface polarization of -0.6 V. (**c**) Photograph of a test device used for this measurement. Scale bar: 0.5 cm.

Yield improvement by transitioning from device- to wafer- level fabrication

To quantify variability and device yield, batches of devices comprising 8 electrodes were fabricated. The manufacturing process was conceptually divided into blocks corresponding to the fabrication of the substrate, encapsulation assembly, screen printing of the electrode coating and implant packaging (connectorization and sealing of the wires). For each process block, the step yield is defined as the ratio between the number of devices correctly processed and the total number of devices processed. Cumulative yield is then defined for each step as the product of the step yield values of all the process steps until the step under analysis. The device yield values reported are cumulative yields at the final packaging step for each of the

process generations. Exclusion criteria to discard misprocessed devices are based on visual inspection for the steps before packaging, as devices are not yet wired and cannot be electrically tested. At the packaging step, devices are considered functional if the modulus of the electrochemical impedance at 1 kHz measured *in vitro* is lower than 10 kΩ for all 8 electrodes on the device.

Three subsequent generations of the process are compared in **Figure S5**. The table of **Figure S5a** summarizes the main changes introduced from one generation of the process to the next, and the graph in **Figure S5b** quantifies the step yield (vertical bars) and cumulative yield (scatter lines). The data is plotted for three batches of 8-electrode arrays, each fabricated following the three different process generations.

Manual process (**Figure 2e**, not shown in **Figure S5**)

In the baseline manual process of **Figure 2e**, implants were built on commercial silicone sheets (.020" NRV G/G 40D 12" X 12", reference 70P001-200-020, Specialty Manufacturing Inc.), cut to shape and laminated on 4" silicon wafers. A 20 µm thick PDMS layer (Sylgard 184) was spin coated on the laminated sheets to enable the deposition of the microcracked Cr/Au interconnect. The interconnect was deposited through a 50 µm thick polyimide mask machined separately and then manually laminated on the PDMS substrate. The encapsulation stack was processed device-by-device by mechanically punching holes in a separate PDMS layer. No yield quantification was attempted for this manual process.

Process Gen. 1, 1 device per wafer

In the first process generation towards a more automated manufacturing, the silicone sheet was replaced by drop casting a 450 µm PDMS membrane on a silicon wafer. A controlled pressure dispenser was used under long working distance dissection binoculars to apply conductive epoxy on wiring pads.

Process Gen. 2, 1 device per wafer

The fundamental improvement introduced in Gen. 2 is the use of laser micromachining to make through-vias in the implant encapsulation, giving access to the embedded gold interconnect. The encapsulation was built with a 20 µm thick layer of PDMS covered by a 23 µm thick PET foil acting as protection and screen print layer for the subsequent application of

the Pt-PDMS coating. During the assembly step, each device was encapsulated by a separate passivation part.

SoS process, 4 devices per wafer

The SoS process is described in detail in **Figure S1** and **Table S1**. The PDMS carrier thickness is split in two identical membranes (substrate and encapsulation), with the interconnect sandwiched in between, on the neutral plane. The PDMS layers are deposited by spin coating. The interconnect pattern mask is laser-machined directly on a PET foil laminated on the PDMS carrier. Substrate and encapsulation are aligned and bonded together at the wafer-level, enabling all the devices in the wafer layout to be passivated in a single step. At present, the SoS process offers a device yield of around 75%.

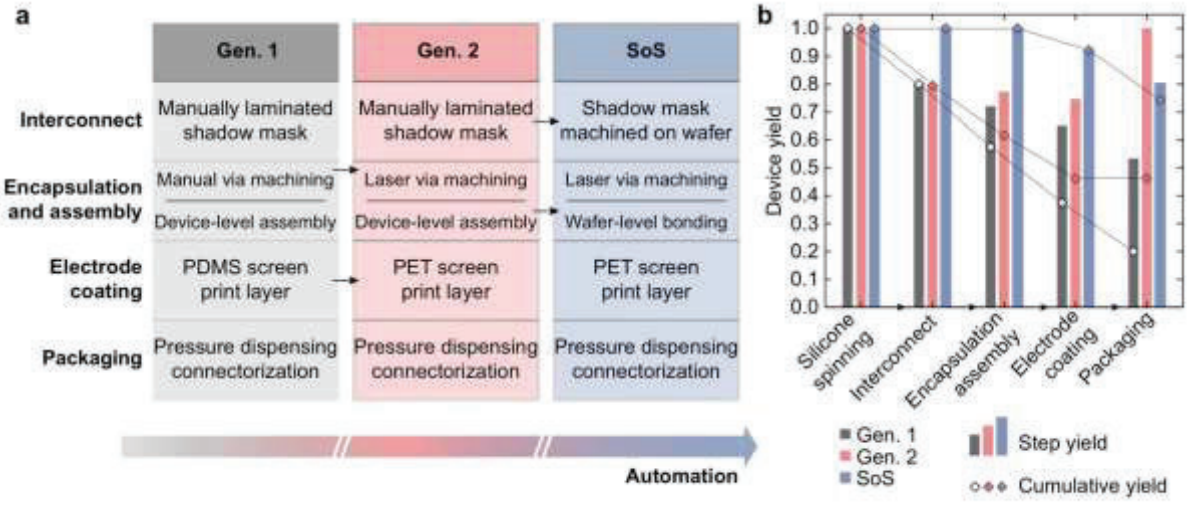

Figure S5 – Transitioning from device- to wafer- level fabrication improves the device yield. (a) Process changes introduced with each subsequent generation of the process. (b) Step and cumulative yield for different process generations. Vertical bars: step yield. Scatter lines: cumulative yield. Starting number of devices: Gen. 1 n = 40, Gen. 2 n = 39, SoS n = 64.

Continuous stimulation and soak tests

The electrical reliability of the Pt-PDMS coating material was evaluated in a continuous stimulation and soak test (**Figure 3a,b,c**). Trains of current-controlled stimulation pulses were applied between test electrodes and a platinum rod counter electrode, immersed in an electrochemical cell containing PBS kept at 37°C in a water bath. Control electrodes were included on the same test device to monitor the passive wear of the electrodes soaked in the same solution as the active electrodes. For this test, a custom-built 8-channel pulse stimulator

was used to deliver charge-balanced, capacitor-coupled monophasic current pulses at an amplitude of 2 mA with cathodic pulse width of 0.3 ms, corresponding to a charge density per phase of about 42 μC cm^{-2}, and at a pulse rate of 400 Hz. The experiment was run until about 1 billion stimulation pulses were injected through the active electrodes.

Electrochemical impedance spectroscopy measurements were taken periodically over time to monitor the evolution of the electrochemical properties of all electrodes. The procedures followed for these measurements are identical to what described in the previous section.

Improved interconnect technology (2Au)

An additional metallization pattern can also be deposited on the encapsulation, in the same way the substrate is processed, in order to double the conductivity of the interconnect and provide a lower overall resistance. When the two gold layers come into contact, these effectively acting as two parallel tracks. Compared to simply depositing a thicker metallization layer, this new approach, which we term 2Au for double gold, offers improved electromechanical reliability when subject to biomimetic strain (**Figure 3e**). **Figure S6** shows a comparison of the electrochemical properties of electrodes built with the two technologies.

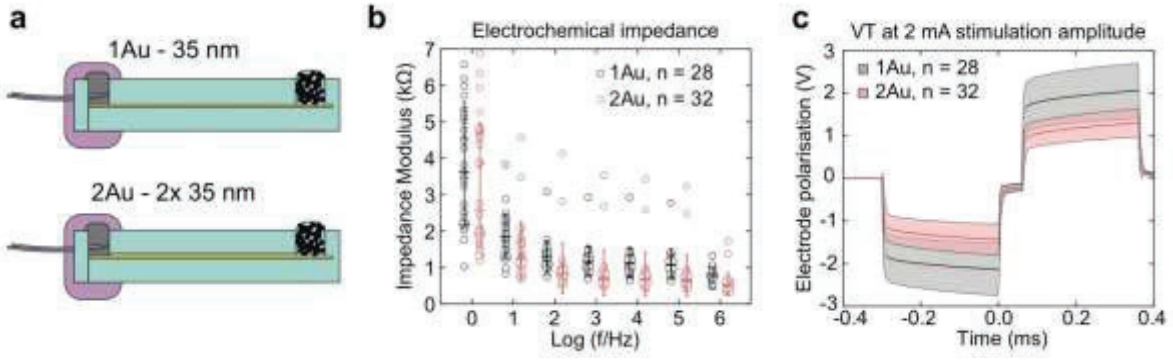

Figure S6 – Electrochemical characterization of electrodes with 1Au and 2Au interconnect technologies. (**a**) Diagram of the sample electrodes, with the 1Au interconnect built as a single 5/35 nm Cr/Au stack, and the 2Au interconnect formed by interfacing 2 such stacks during the assembly process. (**b**) Electrochemical impedance spectrum of a group of electrodes built with the two technologies (GSA: 0.014 cm^2). 1Au: black data points, n = 28 electrodes, whiskers: standard deviation, horizontal bars: median. 2Au: red data points, n = 32 electrodes, whiskers: standard deviation, horizontal bars: median. (**c**) Voltage transient curves for 1Au and 2Au electrodes following current-controlled pulsing in PBS (2 mA, 0.3 ms cathodic pulse width). Data points: mean, shaded areas: standard deviation. 1Au: black data points, n = 28 electrodes. 2Au: red data points, n = 32 electrodes.

Scanning Electron Microscopy (SEM) imaging

SEM images were acquired with a Hitachi SU5000 scanning electron microscope using an annular detector and a beam energy of 4 keV.

Biomimetic multimodal platform and test protocol

Fabrication of the anatomical mock-up models

Cervical vertebrae and spinal cord were directly reconstructed from a Computed Tomography (CT) scan acquired from a macaca fascicularis monkey. STereoLithography (STL) model files were generated, post-processed, and used to 3D print a 1:1 Acrylonitrile Butadiene Styrene (ABS) model of the individual vertebrae, which were then dip-coated with silicone and assembled together using suture treads through the lateral aspects.

A rigid ABS model of the spinal cord was 3D-printed and used as positive mold around which PDMS was cast. After curing, the ABS is extracted from the PDMS to form a cavity in the shape of the cervical spinal cord. This mold was then filled with a polyacrylamide hydrogel that mimics the mechanical properties of the spinal cord (elastic modulus around 1 kPa).[3]

Once polymerized, the hydrogel was removed from the mold and fixed longitudinally on a rotating shaft mounted on a motorized rig. A layer of silicone (ELASTOSIL® M 4600 A/B, Wacker) was deposited on the hydrogel model to mimic the dura mater (elastic modulus ~ 1 MPa) enveloping the spinal cord, while the device rotates. This procedure ensures the deposition of a uniform silicone coating on the hydrogel, with a thickness that can be adjusted by setting the rotation speed of the motor (around 200 µm for this work).

The spinal cord is inserted in the spinal canal, with the silicone coating of the vertebrae and dura mater in contact and holding the parts in place. The device under test is then inserted in the dorsal epidural space, between the vertebrae and the spinal cord model, mimicking a real-life implantation.

Evaluation of the vertebral displacement

We acquired T1-weighted Magnetic Resonance Imaging (MRI) datasets of the cervical segments (vertebral levels C2 to T1) of the same animal, to quantify the physiological deformation of the cervical spinal cord during normal movement. A first MRI scan was acquired with the animal placed in the scanner so as to keep the vertebral column as parallel as possible to the longitudinal axis of the scanner (rest position). We subsequently displaced

the head of the animal at its maximum movement range and we acquired a second dataset (max strain position). In both datasets, we identified eight anatomical landmarks for each spinal segment. By comparing the landmark coordinates extracted from the scans, we observed negligible rotational and translational displacements for vertebral level T1. We therefore assumed vertebral level T1 to be a fixed no-strain element, and we calculated the rigid roto-translational transformation that converts the coordinates of the C2 landmarks in the rest position into the C2 coordinates at max strain position, relative to the landmark coordinates at segment T1.

Design of the biomimetic platform

To reproduce cyclically the spatial displacement described by the vertebral roto-translational transformation, we have designed a dedicated Stewart Platform, a 6 Degrees Of Freedom (6DOF) mechanism that can apply displacement to a mobile surface along and around three axes (X, Y, Z, roll, pitch, yaw).[4] The bottom plate is stationary and is used as a reference plane, while the mobile top plate is moved to reach the desired position by varying the extension of the kinematic legs. A control system that uses a microcontroller to solve the kinematic equations translating the desired movement (input coordinates) into servo commands was developed. Once the platform was assembled, the anatomical model of the implantation was connected with the base of vertebral level T1 fixed to the stationary platform base, the top of vertebral level C2 fixed to the moving top plate, and the implant under test with the lead exiting the spine. The anatomical model is contained in a sealed Plexiglass chamber at the center of the platform filled with saline solution (PBS), so that electrical measurements can be taken concurrently with mechanical tests. The entire system is placed in an incubator set to 37°C and connected to stimulation and measurement equipment.
The input data to set the desired end-position are the movements along three axes (x, y, z) and the rotation around the three axes (roll, pitch, yaw). The motion of the mobile plate is back-sensed with a feedback loop implemented to provide accurate positioning.

Test protocol

Based on the anatomical information, we cyclically applied a set displacement using coordinates corresponding to about 50% of the maximum strain displacement calculated with the roto-translational transformation of the MRI-extracted coordinates. Larger displacements were avoided due to size and performance limitations in the components used to build the platform. The prescribed displacement was repeatedly applied for up to 1 million cycles to the

anatomical model. Physiological-alike mechanical strain was transferred to the epidural implant in a wet ionic environment at 37°C, while simultaneously applying electrical stimulation.

The mechanical cycling was periodically paused to enable electrochemical characterization of the implant under test while still in the platform. EIS and VT measurements were acquired at different time points to monitor the functionality of the electrodes. The functional electrode count during the test (diamond data points in **Figure 3e**) was calculated using the following exclusion criterion for failed electrodes: electrodes were not considered functional when the access voltage (E_{min} - E_{mc}) identified by VT measurements at 2 mA was lower than -10 V in the cathodic phase (indicating an excessive increase of the interconnect resistance).

The dominant failure mechanism observed in single-layer stretchable gold interconnects is the formation of transversal cracks that interrupt the electrical continuity of the tracks (see micrograph in **Figure S7** below).

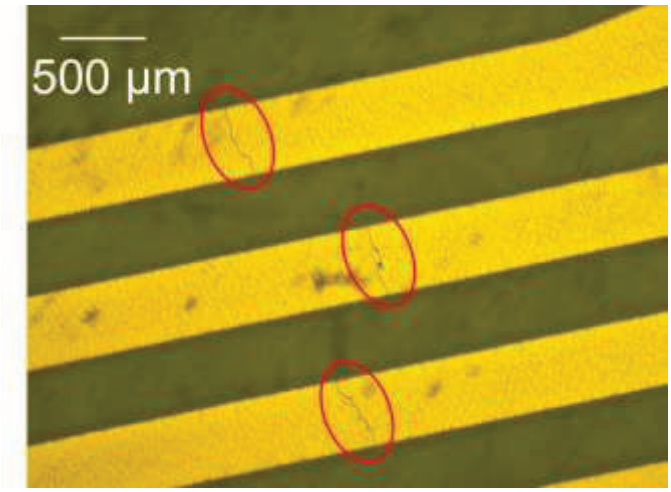

Figure S7 – Failure mode of stretchable gold interconnects. Example of complete transversal crack formation in a single-layer Cr/Au interconnect implant subjected to fatigue testing in the biomimetic multimodal platform.

The test results obtained with the biomimetic platform revealed that thicker gold interconnects (50 nm), while offering a gain in sheet resistance, lose mechanical performance when subject to prolonged fatigue testing. Conversely, the 2Au interconnect technology mitigated this failure mode and exhibited better reliability (**Figure 3e**).

Sterilization

Compatibility with three different sterilization methods was tested: EThylene Oxide (ETO) vapor treatment, autoclave, and hydrogen peroxide (H_2O_2) plasma. For all tests, EIS measurements and SEM scans of the electrode coating were taken after fabrication of the implants and after sterilization, to evaluate any evident effect of the treatment on the implant properties (**Figure S8**). Before sterilization, the implants are packed in bespoke Petri dishes and placed in sterilization bags.

Sterilization parameters

ETO: 100 L ETO sterilization chamber, 3M, Geneva University Hospitals; 55°C, 1 hour exposure to 100 g of ETO vapor, then degas for 48 hours in a ventilated cabinet.

Autoclave: 23 L autoclave system, Systec DB-23, 120°C, 20 min.

H_2O_2 plasma: vaporized H_2O_2 plasma, PlazMax Line P50, Tuttnauer Schweiz, 55°C, 40min.

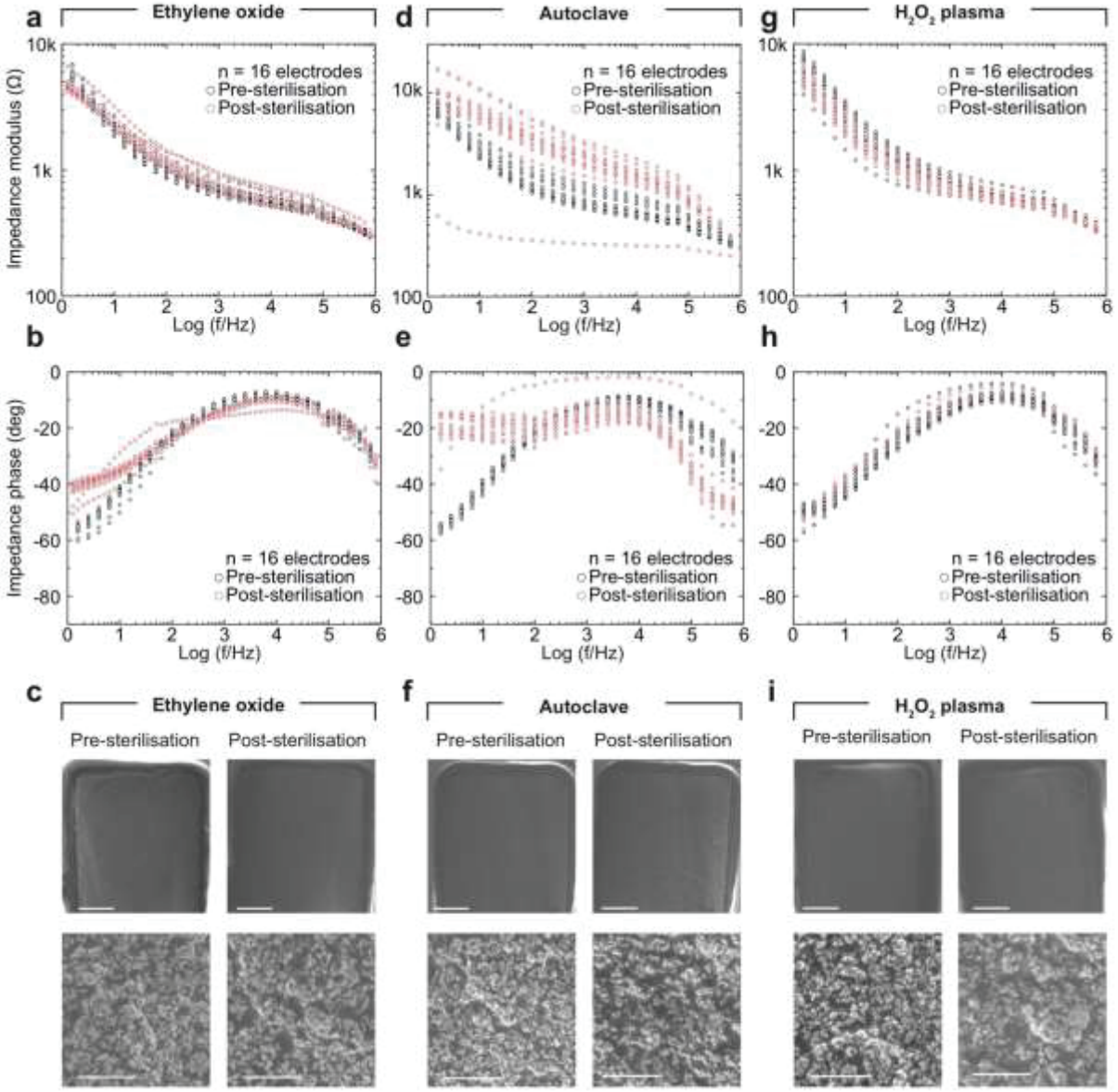

Figure S8 – Effect of sterilization on implant performance. Electrochemical impedance spectra and SEM scans of the electrode coatings acquired pre- and post- sterilization by ETO (**a-c**), autoclave (**d-f**), and H_2O_2 plasma (**g-i**). All data points are shown. Scale bars for the SEM scans: top row – 200 μm; bottom row: 2 μm.

Magnetic Resonance Imaging (MRI) of implants in phantoms

MRI images were acquired with a 3.0 Tesla scanner (SIEMENS MAGNETOM Prisma). For imaging, a test implant was positioned in the center of a circular beaker, sandwiched between two 20 mm thick slabs of agarose gel (agar powder mixed in deionized water, 3% w/w, Agar Agar Patissier). The array was positioned to be in the central axis of the MRI scanner. A clinical spinal cord stimulation electrode array with 16 electrodes (Medtronic) was used for

comparison. T1- and T2- weighted sequences were used for the artefact observation, using the parameters listed in **Table S2**.

The imaging data was exported from the MRI in DICOM format and post-processed using the imaging viewer Osirix Lite (Pixmeo). The images were aligned so the implant lies on the *x-z* plane (MRI referential coordinate system). After adjusting the brightness and contrast, the images were exported without any further processing. **Figure S9** illustrates the sample preparation and positioning, and shows the imaging for the T2 sequence. T1 imaging results are shown in **Figure 3g**.

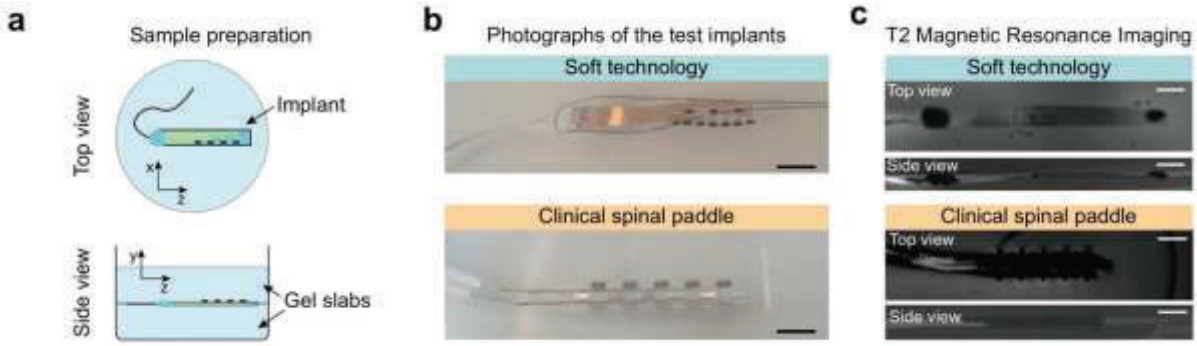

Figure S9 – MRI scan of implants in gel phantom. (**a**) Diagram of the sample preparation. The implant to be imaged is sandwiched between two slabs of gel in a beaker that is placed in the MRI scanner. The referential coordinate system is indicated. (**b**) Photographs of the experimental (top) and clinical (bottom) spinal implants used for imaging. Scale bars: 1 cm. (**c**) Experimental (top) and clinical (bottom) implants imaged with a T2 MRI sequence. Scale bars: 1 cm.

Animal husbandries

Summary table

Animal ID	**Husbandry**	**License number**	**Spinal placement**	**EMG electrodes**
Mk-Ca	UniFr*	2014_42E_ FR	Cervical	Percutaneous
Mk-Li	UniFr	2017_03_ FR	Cervical	Percutaneous
Mk-Cs	UniFr	2017_04E_ FR	Cervical	Tunneled
NHP4	Motac**	LQ16005	Lumbar (rostral)	-
NHP5	Motac	LQ16005	Lumbar (caudal)	-

**University of Fribourg, Switzerland;*

*** Motac Neuroscience Ltd., United Kingdom, operated in Beijing, China*.

Animals used in the acute electrophysiology experiments

The data were collected in 3 adult macaca fascicularis monkeys (2 females – Mk-Ca and Mk-Cs – aged between 7 and 12 years old and weighing between 4 kg and 6 kg; and 1 male – Mk-Li – 16 years old and weighting 7.6 kg). The animals were housed in groups in the facility based at the University of Fribourg, Switzerland, in 45 m^3 rooms with different enrichment features, including an outdoor space and free access to water (see www.unifr.ch/spccr/about/housing).

All surgical and behavioral procedures were approved by the local ethical committee in accordance with the guidelines for the Care and Use of Laboratory Animals and approved by local (Canton of Fribourg) and federal (Swiss) veterinary authorities with authorization numbers 2014_42E_FR (Mk-Ca), 2017_03_FR (Mk-Li), 2017_04E_FR (Mk-Cs).

Animals used in the 6-week implantation experiments

Experiments were approved by the Institutional Animal Care and Use Committee of Bordeaux (CE50, France) and performed in accordance with the European Union directive of 22 September 2010 (2010/63/EU) on the protection of animals used for scientific purposes in an AAALAC-accredited facility (Chinese Academy of Science, Beijing, China). Two healthy male macaque monkeys (macaca fascicularis, NHP4 and NHP5) weighing about 5 kg were used for the experiment.

Surgical procedures

Animals used in the acute electrophysiology experiments

During all surgeries, the animals were kept in deep anesthesia (induction with ketamine (10 mg kg^{-1}) and midazolam (0.110 mg kg^{-1}) administered intramuscularly, and maintained with continuous intravenous infusion of fentanyl (0.1 – 0.7 µg kg^{-1} min^{-1}) and Propofol (0.1 – 0.4 mg kg^{-1} min^{-1}). Oxygen supply was provided by means of a nasal tube and heart rate, respiration rate, body temperature and blood oxygenation were continuously monitored throughout the procedures.

A dorsal mid-line skin incision is made at the desired vertebral level, and the muscles covering the laminae are retracted. Complete flavectomies (removal of the ligament) and laminectomies are performed at the insertion and exit points of the vertebral column. A soft silicone guiding tool is inserted epidurally following the midline, from the insertion laminectomy to the exit laminectomy, caudal to rostral. The tip of the electrode array is then anchored to the tail of the guiding tool, which is pulled to slide the implant into the epidural space.

To record electromyographic signals in animal Mk-Cs, bipolar electrodes were prepared by trimming a small section of insulation from Teflon-coated stainless steel wires (AS631, Cooner Wire). Pairs of electrode wires plus a ground wire are tunneled from the location of the target muscles to a custom-built cranial pedestal fixed on the skull. The EMG wires are terminated to a multipolar connector (Omnetics Connector Corporation) embedded in the pedestal, enabling the electrical connection to external recording equipment. For the additional cervical electrophysiology experiments (**Figure S10**), the EMG data was instead acquired with percutaneous needle electrodes acutely inserted in the targeted muscles.

Animals used in the 6-week implantation experiments

Surgical procedures were performed under full anesthesia induced with atropine (0.04 mg kg^{-1}) and ketamine (10 mg kg^{-1}, intramuscular injection) and maintained under 1% – 3% isoflurane after intubation. A certified functional neurosurgeon supervised all the surgical procedures. One of the two monkeys received an epidural electrode array inserted at the L4-L5 vertebral level, while the second monkey had an epidural electrode array implanted at the L6-L7 vertebral level. The implants prepared for this study were wired to clinical 8-polar leads. After implantation, the connector end was protected with a mating female connector that was left under the skin.

A skin incision at days 15 and 43 (week 2 and week 6) post-implantation was performed under light anesthesia to access the lead connector and take stimulation and impedance measurements. At the end of each session, the leads were folded and placed back under the skin in the most natural position, and the subcutaneous incision was closed again with suture points.

In vivo electrochemical characterization

Electrochemical Impedance Spectroscopy (EIS)

EIS measurements of implanted electrodes were taken with the same equipment and in the same configuration as *in vitro* measurements. Two separate needle electrodes were inserted percutaneously in the skin on either side of the spine to serve as counter and reference electrodes.

Muscle Recruitment Curves (RC)

Epidural Electrical Stimulation (EES) was delivered through charge-balanced biphasic, asymmetric, cathodic-leading, 1:5 cathodic:anodic amplitude ratio current pulses at a cathodic pulse width of 0.3 ms, using a Tucker-Davis technologies neural stimulation and recording rack. Stimulation trains were delivered to the spinal cord through the different electrodes on the spinal arrays, eliciting motor responses in the muscles implanted with EMG electrodes. For each electrode, the minimum stimulation amplitude necessary to elicit a motor response (referred hereafter as motor threshold) and the amplitude at which all motor evoked potentials were saturated (referred hereafter as saturation amplitude) were identified by observing the recorded EMG signals. This procedure defines the stimulation current limits. Subsequently, trains of stimulation pulses of 11 increasing amplitude levels ranging from motor threshold to saturation were delivered at 1.5 Hz pulse rate (4 trials per amplitude level), while recording the EMG activity. The recorded EMG signals were sampled at 12 kHz, band-pass filtered (30 Hz – 800 Hz) and normalized to the maximum activity recorded across the responses of all the muscles obtained by stimulating from a specific electrode of the spinal array. The muscle recruitment level was evaluated by calculating the peak-to-peak amplitude of the triggered EMG signals immediately following the stimulation pulse. Recruitment curves were built by plotting the level of muscle recruitment (4 trials) as a function of the stimulation current amplitude.

Visual detection of threshold and maximum contraction amplitudes and measurement of the minimum cathodic polarization

In the 6-week study, at each of the 3 time points EES was delivered through the electrodes implanted in the lumbar epidural space. Charge-balanced biphasic, symmetric, cathodic-leading current pulses of 0.3 ms pulse width were injected through each implanted electrode at a pulse rate of 1 Hz, using an A-M Systems 2100 Isolated Pulse Stimulator. Two percutaneous needles were placed in the skin on either side of the spine, acting as separate counter and refence electrodes.

EES was delivered sequentially through each electrode with increasing current amplitude, with the aim of identifying the minimum amplitude of the stimulation current at which motor responses are visually detected (hereinafter named motor threshold), and the current amplitude at which the motor response is maximum (no increased response was detected when the stimulation amplitude was increased, or excessive contractions elicited that destabilized the animal). For both animals and at each time point, the motor threshold and maximum contraction amplitudes were assessed visually by a specialized veterinary, driving the stimulation amplitude in the 0 – 10 mA range.

Voltage transient curves were recorded during stimulation at the threshold and maximum contraction amplitudes, using an oscilloscope (TBS1202B Digital storage oscilloscope, Tektronix) connected to the positive output of the stimulator and to the reference percutaneous needle electrode. The minimum cathodic polarization (E_{min}) was assessed as the minimum voltage recorded with a VT measurement at a specific stimulation amplitude.

Repeatability of the selective muscle recruitment for cervical EES

The cervical electrophysiology experiment shown in **Figure 4** was repeated with a total of three NHPs in independent sessions, with the aim of verifying that our designs and protocols enable reproducible results regardless of the inter-subject anatomical differences and the variability in the implant placement. Muscle recruitment curves were acquired in three animals using two different electrode layouts, as shown in **Figure S10**. The results highlight that in all cases we were able to select stimulation electrodes eliciting similar muscle responses, with the selective activation of the biceps, triceps and abductor pollicis. This is a promising demonstration that further validates the viability of our technology for use in the clinical contexts of rehabilitation and brain-machine interfaces, where selective stimulation targets are desirable.

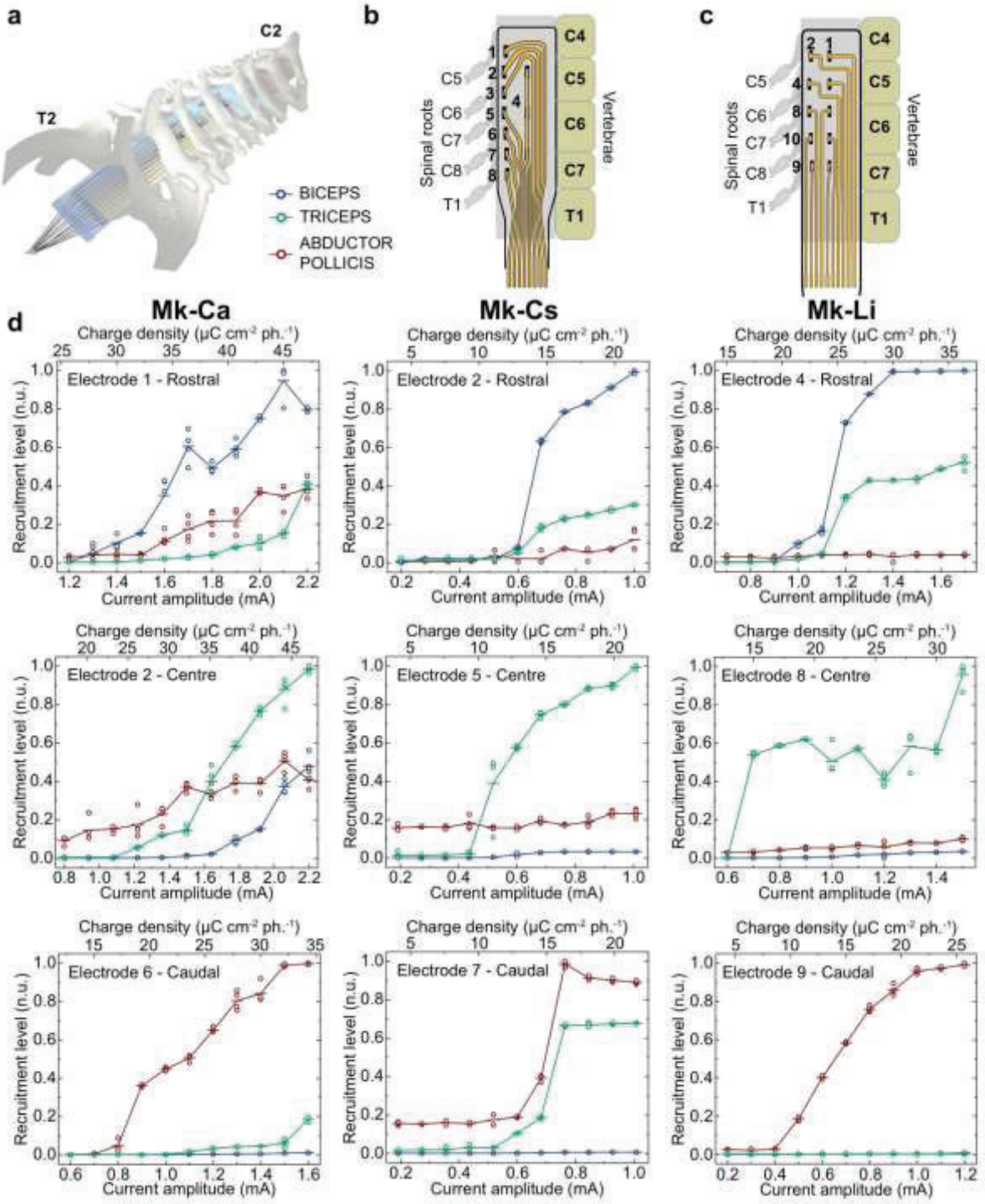

Figure S10 – Selective muscle recruitment in repeated electrophysiology experiments with three different NHPs. (**a**) Diagram of the placement of the electrode array in the cervical epidural space. (**b**) Schematic overlay of the implant layout used for animals Mk-Ca and Mk-Cs on the cervical vertebral segments. (**c**) Schematic overlay of the implant layout used for Mk-Li on the cervical vertebral segments. (**d**) Selective activation of the biceps (blue, arm flexor), triceps (green, arm extensor), and abductor pollicis brevis (red, thumb abductor)

using EES in three different animals. Each data point corresponds to an individual trial out of a total of 4 trials per current amplitude per electrode. Horizontal bars: mean.

Stability of the implant performance in vivo

In the 6-week implantation study illustrated in **Figure 4**, the functionality of electrode arrays implanted in the lumbar epidural space was verified in two separate monkeys. The layout and interconnect arrangement of the two implants used for this study are illustrated in **Figure S11**.

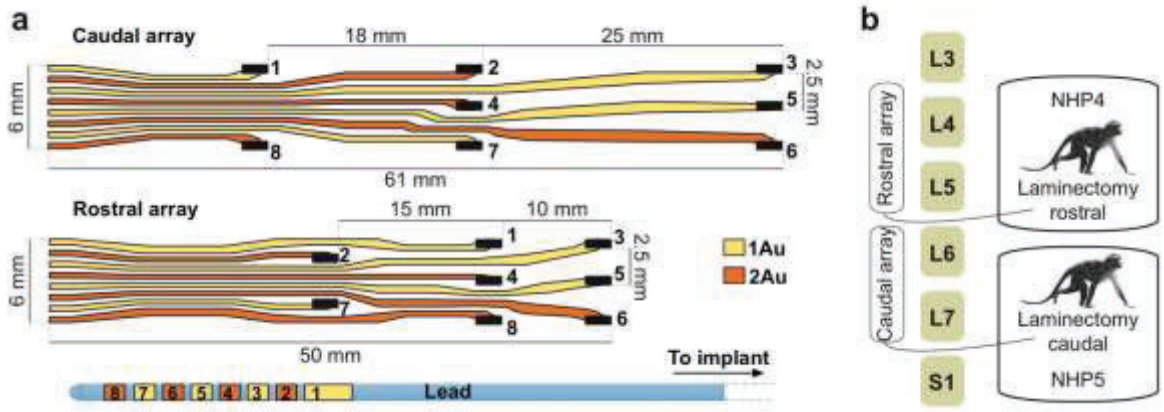

Figure S11 – (**a**) Layout of the implanted electrode arrays with alternate single- and double-interconnect technology. (**b**) Diagram of the placement of the two arrays in the two animals.

The electrode arrays explanted from the animals used for the 6-week implantation experiment were examined by measuring the impedance spectrum of all electrodes and imaging the coating by SEM (**Figure S12**). With the exception of 2 out of 16 electrodes in the rostral implant, the impedance spectra confirm that no significant change has occurred between post-fab and post-explantation (**Figure S12a-f**). Comparison with the data points collected *in vivo* at 6 weeks suggests however that 1 of the 2 high-impedance electrodes have failed during explantation, handling and/or shipping of the device.

Additional SEM scans of the coating on different electrodes are provided in **Figure S12g**. Representative areas of the electrode coating are shown, from left to right, with limited biological residue, irregularities in the morphology, and sparser density of Pt particles at the surface. These images provide qualitative yet convincing evidence that the electrodes have not undergone significant change during the 6-week implantation period, confirming what already shown quantitatively by the electrochemical impedance data.

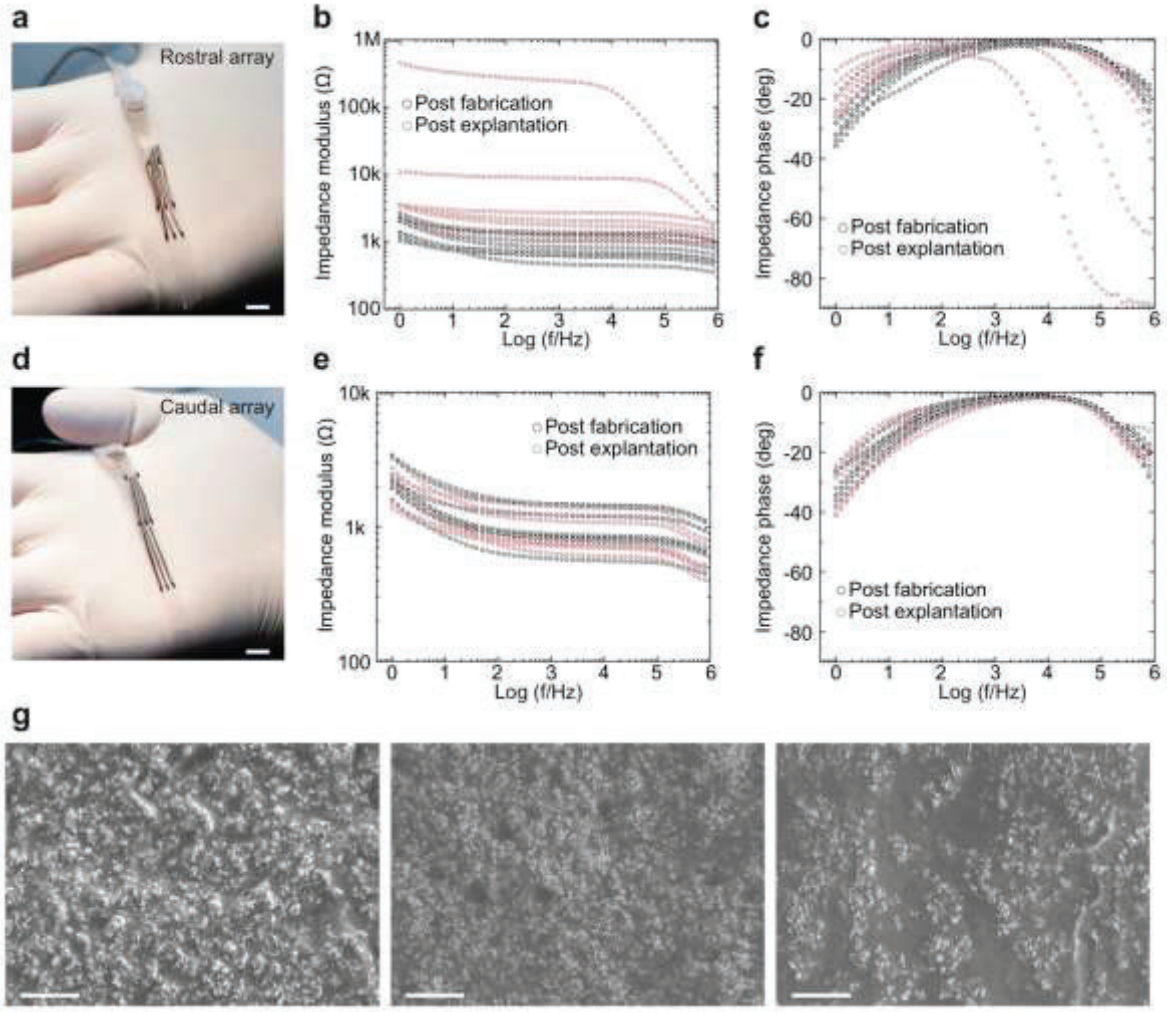

Figure S12 – Characterization of the electrode arrays explanted after 6 weeks in NHPs. Photographs and impedance spectra (modulus and phase) of the lumbar arrays (rostral, **a-c**; caudal, **d-f**) extracted after 6 weeks implantation in NHPs. Scale bars: 1 cm. Impedance spectra post-fabrication and post-explantation are compared, with all data points shown (n = 8 electrodes per array). (**g**) SEM scans of the Pt-PDMS coating at three different electrodes on the explanted devices. Scale bars: 2 μm.

Statistical analysis

Individual data points are reported for all displayed quantifications, unless otherwise stated.

Table S1 – SoS process steps. Description and parameters.

Substrate			
Step	**Process**	**Materials**	**Parameters**
a	4” silicon carrier, surface activation by oxygen plasma	100 mm silicon wafer, single side polished, 525 ± 25 µm thick, Siegert Wafer	Plasma: - Power 30 W - O_2 flow 20 sccm - Time 30 s
b	1. Spin coating of PolyStyrene Sulfonic acid water-release layer 2. Baking on a hotplate	Poly(4-styrenesulfonic acid) solution, Sigma Aldrich	Spin: 2000 rpm, 45 s Bake: 150°C, 1 min
c	1. Mixing PolyDimethylSiloxane, 10:1 wt pre-polymer:cross-linker 2. Spin coating of 170 – 220 µm PDMS substrate carrier 3. Baking in a temperature-controlled oven	PDMS, Sylgard 184, Dow Corning	Spin: 150 – 320 rpm, 1 min Cure: 75°C, 3 hours
d	Lamination of 23 µm PolyEthylene Terephtalate shadow mask film	PET foil, Dupont Mylar 23A, Lohmann	Cold lamination
e	1. Laser machining of the PET mask 2. Removal of the PET patterns to expose the PDMS surface	-	Optec femtosecond excimer laser
f	Thermal evaporation of the interconnect metallisation, 5 nm chromium and 35 nm gold	Chrome-plated tungsten rod, Kurt J. Lesker Company Ltd. Gold pellets, 1-3 mm diameter, 99.99% purity, Metalor Technologies SA	Vacuum: ~ 2e-6 mbar Evaporation rates: - Chromium ~ 0.3 Å/s - Gold ~ 1.1 Å/s
g	Lift-off by peeling off the PET shadow mask to reveal the interconnect patterns	-	-
h	PDMS surface activation by oxygen plasma	-	Plasma: - Power 30 W - O_2 flow 20 sccm - Time 30 s

Encapsulation			
Step	**Process**	**Materials**	**Parameters**
a	4” silicon carrier	100 mm silicon wafer, single side polished, 525 ± 25 µm thick, Siegert Wafer	-
b	1. Mixing PolyDimethylSiloxane, 10:1 wt pre-polymer:cross-linker 2. Spin coating of ~ 50 µm PDMS handling layer 3. Baking in a temperature-controlled oven	PDMS, Sylgard 184, Dow Corning	Spin: 1000 rpm, 1 min Cure: 75°C, 3 hours
c	Lamination of 23 µm PolyEthylene Terephtalate handling film	PET foil, Dupont Mylar 23A, Lohmann	Cold lamination

d	1. Mixing PolyDimethylSiloxane, 10:1 wt pre-polymer:cross-linker 2. Spin coating of ~ 170 – 220 µm PDMS encapsulation layer 3. Baking in a temperature-controlled oven	PDMS, Sylgard 184, Dow Corning	Spin: 150 – 320 rpm, 1 min Cure: 75°C, 3 hours
e	Lamination of 23 µm PolyEthylene Terephtalate shadow mask film	PET foil, Dupont Mylar 23A, Lohmann	Cold lamination
f	1. Laser machining of the PET mask 2. Laser machining of the PET/PDMS/PET stack 3. Removal of the PET patterns to expose the PDMS surface	-	Optec femtosecond excimer laser
g	*Only for double-interconnect (2Au) devices* Thermal evaporation of the interconnect metallisation, 5 nm chromium and 35 nm gold	Chrome-plated tungsten rod, Kurt J. Lesker Company Ltd. Gold pellets, 1-3 mm diameter, 99.99% purity, Metalor Technologies SA	Vacuum: ~ 2e-6 mbar Evaporation rates: - Chromium ~ 0.3 Å/s - Gold ~ 1.1 Å/s
h	Lift-off by peeling off the PET shadow mask to reveal the interconnect patterns	-	-
i	Removal of the encapsulation from the silicon carrier by peeling off the stack from the bottom PET handling layer	-	-
j	1. Flexible, transparent acrylic disc carrier 2. Spin coating of PDMS handling layer (identical to step **encapsulation b**) on disc 3. Transfer the encapsulation stack to the disc carrier	100 mm ø clear cast acrylic disc, 1 mm thickness, polished, Simply Plastics PDMS, Sylgard 184, Dow Corning	Spin: 1000 rpm, 1 min Cure: 75°C, 3 hours
k	PDMS surface activation by oxygen plasma	-	Plasma: - Power 30 W - O_2 flow 20 sccm - Time 30 s

Assembly

Step	Process	Materials	Parameters
a	1. Mounting plasma-treated substrate and encapsulation carriers on an alignment rig 2. Optical alignment of substrate and encapsulation on a *x-y-theta* stage	-	-
b	Covalent bonding between the top PDMS surfaces of the substrate and encapsulation by physical contact	-	-
c	Removal of the encapsulation carrier by peeling off the acrylic disc	-	-
d	Oxygen plasma treatment to activate the exposed PDMS surface in the vias	-	Plasma: - Power 20 W - Base pressure ~ 0.4 mbar - O_2 pressure ~ 0.2 – 0.4 mbar - Time 30 s

e	1. Preparation of the electroactive composite coating by dispersing platinum particles in a PDMS matrix (70% weight ratio Pt:PDMS) diluted in cyclohexane (2:1 weight ratio Cyclohexane:PDMS) 2. Screen printing of the composite coating into the electrode vias	Platinum powder, 99.9% purity, avg. particle size 0.27 – 0.47 µm, Strem Chemicals, Inc. PDMS, Sylgard 184, Dow Corning Cyclohexane, ≥99.8% Laboratory Reagent, Sigma Aldrich	-
f	Peeling off the PET screen print layer to define the coated electrode areas	-	-
g	1. Wait overnight for the solvent in the composite to degas and for the coating to completely flow in the electrode vias 2. Baking in a temperature-controlled oven for the polymerisation of the composite coating	-	Cure: 55°C, 4 hours after waiting overnight
h	1. Cut the PDMS stacks to the desired implant shape 2. Cut the edge of the interconnect vias	-	-

Packaging

Step	Process	Materials	Parameters
a	1. Casting and curing ~ 3 mm thick PDMS membrane 2. Mechanical punching of the membrane on a *x-y* stage, to make rows of holes at a pitch matching the interconnect pads 3. Thread electrical wires through the holes in the membrane 4. Strip the insulation off the wires 5. Place the soft connector over the interconnect pads	PDMS, Sylgard 184, Dow Corning AS631 multistranded stainless steel wire, Cooner Wire TiN coated stainless steel punch, 0.33 mm cutting edge diameter, Syneo	PDMS curing: 75°C, 3 hours Hole punching: 330 µm diameter 8 – 10 holes 0.8 – 1 mm pitch
b	Pressure dispensing of conductive epoxy into the pad vias to connect the wires to the interconnect	Epotek H27D electrically conductive silver epoxy, part A	Needle gauge: 25G Pressure: ~ 5.5 bar
c	Mechanical stabilisation of the connector by dispensing Room-Temperature-Vulcanising silicone adhesive	One component silicone sealant 734 clear, Dow Corning	Setting time: 4 hours
d	Releasing the implants from the silicon carrier by dissolving the PSS release layer in deionised water	-	-
e	Mechanical stabilisation and electrical insulation of the connector back and sides by dispensing Room-Temperature-Vulcanising silicone adhesive	One component silicone sealant 734 clear, Dow Corning	Setting time: 4 hours

Table S2 – Magnetic Resonance Imaging parameters.

T1 Sequence parameters

SIEMENS MAGNETOM Prisma

TA: 4:44 PM: FIX Voxel size: 1.0×1.0×1.0 mmPAT: 2 Rel. SNR: 1.00 : tfl

Properties

Prio recon	Off
Load images to viewer	On
Inline movie	Off
Auto store images	On
Load images to stamp segments	Off
Load images to graphic segments	Off
Auto open inline display	Off
Auto close inline display	Off
Start measurement without further preparation	Off
Wait for user to start	On
Start measurements	Single measurement

Routine

Slab group	
Slabs	1
Dist. factor	50 %
Position	R1.8 A13.5 F30.5 mm
Orientation	Sagittal
Phase enc. dir.	A >> P
AutoAlign	Head > Brain
Phase oversampling	0 %
Slice oversampling	15.4 %
Slices per slab	208
FoV read	256 mm
FoV phase	100.0 %
Slice thickness	1.00 mm
TR	2300.0 ms
TE	2.25 ms
Averages	
Concatenations	
Filter	Prescan Normalize
Coil elements	HC1-7;NC1,2

Contrast - Common

TR	2300.0 ms
TE	2.25 ms
Magn. preparation	Non-sel. IR
TI	900 ms
Flip angle	8 deg
Fat suppr.	None
Water suppr.	None

Contrast - Dynamic

Averages	
Averaging mode	Long term
Reconstruction	Magnitude
Measurements	1
Multiple series	Each measurement

Resolution - Common

FoV read	256 mm
FoV phase	100.0 %
Slice thickness	1.00 mm
Base resolution	256
Phase resolution	100 %
Slice resolution	100 %
Phase partial Fourier	7/8
Slice partial Fourier	7/8
Interpolation	Off

Resolution - iPAT

PAT mode	GRAPPA
Accel. factor PE	2
Ref. lines PE	24
Accel. factor 3D	
Reference scan mode	Integrated

Resolution - Filter Image

Image Filter	Off
Distortion Corr.	Off
Prescan Normalize	On
Unfiltered images	Off
Normalize	Off
B1 filter	Off

Resolution - Filter Rawdata

Raw filter	Off
Elliptical filter	Off

Geometry - Common

Slab group	
Slabs	
Dist. factor	50 %
Position	R1.8 A13.5 F30.5 mm
Orientation	Sagittal
Phase enc. dir.	A >> P
Slice oversampling	15.4 %
Slices per slab	208
FoV read	256 mm
FoV phase	100.0 %
Slice thickness	1.00 mm
TR	2300.0 ms
Multi-slice mode	Single shot
Series	Ascending
Concatenations	1

Geometry - AutoAlign

Slab group	1
Position	R1.8 A13.5 F30.5 mm
Orientation	Sagittal
Phase enc. dir.	A >> P
AutoAlign	Head > Brain
Initial Position	R1.8 A13.5 F30.5
R	1.8 mm
A	13.5 mm
F	30.5 mm
Initial Rotation	-9.53 deg
Initial Orientation	Sagittal

Geometry - Navigator

System - Miscellaneous

Positioning mode	FIX
Table position	H
Table position	0 mm
MSMA	S - C - T
Sagittal	R >> L
Coronal	A >> P
Transversal	F >> H
Coil Combine Mode	Adaptive Combine
Save uncombined	Off

System - Miscellaneous

Matrix Optimization	Off
AutoAlign	Head > Brain
Coil Select Mode	Off - AutoCoilSelect

System - Adjustments

B0 Shim mode	Tune up
B1 Shim mode	TrueForm
Adjust with body coil	Off
Confirm freq. adjustment	Off
Assume Dominant Fat	Off
Assume Silicone	Off
Adjustment Tolerance	Auto

System - Adjust Volume

Position	Isocenter
Orientation	Transversal
Rotation	0.00 deg
A >> P	263 mm
R >> L	350 mm
F >> H	350 mm
Reset	Off

System - pTx Volumes

B1 Shim mode	TrueForm
Excitation	Non-sel.

System - Tx/Rx

Frequency 1H	123.257291 MHz
Correction factor	1
Gain	Low
Img. Scale Cor.	1.000
Reset	Off
? Ref. amplitude 1H	0.000 V

Physio - Signal1

1st Signal/Mode	None
TR	2300.0 ms
Concatenations	1

Physio - Cardiac

Magn. preparation	Non-sel. IR
TI	900 ms
Fat suppr.	None
Dark blood	Off
FoV read	256 mm
FoV phase	100.0 %
Phase resolution	100 %

Physio - PACE

Resp. control	Off
Concatenations	1

Inline - Common

Subtract	Off
Measurements	1
StdDev	Off
Save original images	On

Inline - MIP

MIP-Sag	Off
MIP-Cor	Off
MIP-Tra	Off
MIP-Time	Off

Inline - MIP

Save original images	On

Inline - Composing

Distortion Corr.	Off

Sequence - Part 1

Introduction	On
Dimension	3D
Elliptical scanning	Off
Reordering	Linear
Asymmetric echo	Allowed
Flow comp.	No
Multi-slice mode	Single shot
Echo spacing	6.8 ms
Bandwidth	200 Hz/Px

Sequence - Part 2

RF pulse type	Normal
Gradient mode	Normal
Excitation	Non-sel.
RF spoiling	On
Incr. Gradient spoiling	Off
Turbo factor	210

Sequence - Assistant

Mode	Off

T2 Sequence parameters

SIEMENS MAGNETOM Prisma

TA: 6:56 PM: FIX Voxel size: 0.5×0.5×0.5 mmPAT: Off Rel. SNR: 1.00 : spcR

Properties

Prio recon	Off
Load images to viewer	On
Inline movie	Off
Auto store images	On
Load images to stamp segments	Off
Load images to graphic segments	Off
Auto open inline display	Off
Auto close in ine display	Off
Start measurement without further preparation	Off
Wait for user to start	Off
Start measurements	Single measurement

Routine

Slab group	
Slabs	
Position	R12.7 A28.1 F0.9 mm
Orientation	S > C-29.2 > T- 16.8
Phase enc. dir.	A >> P
AutoAlign	
Phase oversampling	10 %
Slice oversampling	16.7 %
Slices per slab	96
FoV read	153 mm
FoV phase	100.0 %
Slice thickness	0.50mm
TR	1400 ms
TE	98 ms
Averages	1.7
Concatenations	
Filter	Raw filter, Prescan Normalize
Coil elements	HC1-7;NC1,2

Contrast - Common

TR	1400 ms
TE	98 ms
MTC	Off
Magn. preparation	None
Flip angle	120 deg
Fat suppr.	None
Blood suppr.	Off
Restore magn.	On

Contrast - Dynamic

Averages	1.7
Reconstruction	Magnitude
Measurements	1
Multiple series	Each measurement

Resolution - Common

FoV read	153 mm
FoV phase	100.0 %
Slice thickness	0.50 mm
Base resolution	320
Phase resolution	100 %
Slice resolution	50 %
Phase partial Fourier	Allowed
Slice partial Fourier	7/8
Interpolation	Off

Resolution - iPAT

PA	None

Resolution - Filter Image

Image Filter	Off
Distortion Corr.	Off
Prescan Normalize	On
Unfiltered images	Off
Normalize	Off
B1 filter	Off

Resolution - Filter Rawdata

Raw filter	On
Elliptical filter	Off

Geometry - Common

Slab group	
Slabs	1
Position	R12.7 A28.1 F0.9 mm
Orientation	S > C-29.2 > T-16.8
Phase enc. dir	A >> P
Slice oversampling	16.7 %
Slices per slab	96
FoV read	153 mm
FoV phase	100.0 %
Slice thickness	0.50 mm
TR	1400 ms
Series	Ascending
Concatenations	1

Geometry - AutoAlign

Slab group	
Position	R12.7 A28.1 F0.9 mm
Orientation	S > C-29.2 > T-16.8
Phase enc. dir	A >> P
AutoAlign	
Initial Position	R12.7 A28. 1F0.9
R	12.7 mm
A	28.1 mm
F	0.9 mm
Initial Rotation	0.00 deg
Initial Orientation	S > C
S > C	-29.2
> T	-16.8

Geometry - Saturation

Fat suppr.	None
Restore magn.	On
Special sat.	None

Geometry - Navigator

System - Miscellaneous

Positioning mode	FIX
Table position	H
Table position	0 mm
MSMA	S - C - T
Sagittal	R >> L
Coronal	A >> P
Transversal	F >> H
Coil Combine Mode	Adaptive Combine

System - Miscellaneous

Save uncombined	Off
Matrix Optimization	Performance
AutoAlign	---
Coil Select Mode	Off - AutoCoilSelect

System - Adjustments

B0 Shim mode	Tune up
B1 Shim mode	Volume-selective
Adjust with body coil	Off
Confirm freq. adjustment	Off
Assume Dominant Fat	Off
Assume Silicone	Off
Adjustment Tolerance	Auto

System - Adjust Volume

Position	Isocenter
Orientation	Transversal
Rotation	0.00 deg
A >> P	263 mm
R >> L	350 mm
F >> H	350 mm
Reset	Off

System - pTx Volumes

B1 Shim mode	Volume-selective
Excitation	Slab-sel.
pTx Volume	1
Vol. Property	B1 Shim Vol.
Position	R24.5 A4.0 F3.5 mm
Orientation	C > S33.5 > T-2.6
Rotation	-70.69 deg
F >> H	68 mm
R >> L	55 mm
A >> P	51 mm
Vol. Visibility	On

System - Tx/Rx

Frequency 1H	123.257291 MHz
Correction factor	1
Gain	High
Img. Scale Cor.	1.000
Reset	Off
? Ref. amplitude 1H	0.000 V

Physio - Signal1

1st Signal/Mode	None
Trigger delay	0 ms
TR	1400 ms
Concatenations	1

Physio - Cardiac

Magn. preparation	None
Fat suppr.	None
Dark blood	Off
FoV read	153 mm
FoV phase	100.0 %
Phase resolution	100 %

Physio - PACE

Resp. control	Off
Concatenations	1

Inline - Common

Subtract	Off
Measurements	1
StdDev	Off
Save original images	On

Inline - MIP

MIP-Sag	Off
MIP-Cor	Off
MIP-Tra	Off
MIP-Time	Off
Save original images	On

Inline - Composing

Distortion Corr.	Off

Sequence - Part 1

Introduction	On
Dimension	3D
Elliptical scanning	Off
Reordering	Linear
Flow comp.	No
Echo spacing	6.7 ms
Adiabatic-mode	Off
Bandwidth	289 Hz/Px

Sequence - Part 2

Echo train duration	422 ms
RF pulse type	Normal
Gradient mode	Fast
Excitation	Slab-sel.
Flip angle mode	Constant
Turbo factor	98

Sequence - Assistant

Allowed delay	30 s

Supporting Information References

[1] G. Sengul, C. Watson, I. Tanaka, G. Paxinos, *Atlas of the Spinal Cord: Mouse, Rat, Rhesus, Marmoset, and Human*, Elsevier Science, **2012**.
[2] S. F. Cogan, *Annu Rev Biomed Eng* **2008**, *10*, 275.
[3] J. R. Tse, A. J. Engler, *Current Protocols in Cell Biology* **2010**, *47*, 10.16.1.
[4] D. Stewart, *Proceedings of the Institution of Mechanical Engineers* **1965**, *180*, 371.

Supporting Information Video S1

Multimodal biomimetic *in vitro* platform for validation of soft epidural spinal cord implants